ACTA METALLURGICA SLOVACA
2022, VOL. 28, NO. 3, 133-139

RESEARCH PAPER

THERMAL STABILITY AND THERMAL EXPANSION BEHAVIOR OF AlFeCoNiCu AS-CAST HIGH-ENTROPY DUAL-PHASE ALLOY

Vladimir Tsepelev[1], *Kseniya Shmakova*[1*], *Olga Chikova*[1]

[1]Ural Federal University, Mira, 19, Yekaterinburg, Russia

*Corresponding author: k.y.shmakova@urfu.ru, tel.: +79122749946, IFE, Ural Federal University, 620002, Yekaterinburg, Russia

Received: 05.07.2022
Accepted: 01.09.2022

ABSTRACT

This work is devoted to the thermal stability and thermal expansion of dual-phase AlFeCoNiCu as-cast high-entropy alloy of equiatomic composition. The high entropy alloy AlFeCoNiCu is mix of FCC + BCC phases. According to characterized by EDS-analysis, Fe and Co are almost uniformly distributed in both phases in comparison with other elements. The BCC phase is rich in Ni and Al, and the FCC phase is Cu. Our measurement results of hardness and elastic modulus values for inter dendrites (FCC phase) and dendrites (BCC phase) of as-cast AlFeCoNiCu alloy showed the difference between there. Hardness values for inter dendrites and dendrites: 3.4±0.4GPa and 4.1±0.6GPa. Elastic modulus values for inter dendrites and dendrites: 130.5±2.0GPa and 166.5±5.6GPa. The thermal stability of the phases presented in AlFeCoNiCu as-cast high-entropy alloy has been studied with dilatometry and differential scanning calorimetry (DSC). The DSC thermogram shows an endothermic peak at 1000K. The coefficient of thermal expansion (CTE) increases linear from $(10.6 \pm 0.3)\times10^{-6}K^{-1}$ at room temperature to $(27.7 \pm 0.3) \times10^{-6}K^{-1}$ at 370K. The CTE temperature curve also shows the peak at 1000K. The peaks in the CTE temperature and the DSC curve suggest a phase transformation with increasing temperature up to~1000K.

Keywords: AlFeCoNiCu, high-entropy dual-phase alloy, microstructure, differential scanning calorimetry, thermal and phase stability

INTRODUCTION

In recent years, high-entropy alloys (HEAs) have attracted widespread attention. As compared to conventional alloys, the HEAs exhibit excellent properties in terms of strength, wear resistance, thermostable microstructure, oxidation and corrosion resistance [1]. The formation of HEA in the form of alloys with five or more basic elements is possible due to the predominant formation of solid solutions over multiphase microstructures due to the large contribution of configurational entropy to free energy. Two major concepts have been formulated for HEAs, the "entropy effect" [2] and the "sluggish diffusion effect" [3]. The entropy influence on the alloy structure and properties is generalized from the standpoint of thermodynamics, kinetics, and the size and position of atoms. The "sluggish diffusion effect" in the HEAs leads to the low coarsening rate of a solid phase as compared to other conventional alloys. The new transformation-induced plasticity-assisted, dual-phase high-entropy alloy (TRIP-DP-HEA) was recently presented [4]. This alloy combines the best: extensive hardening due to the decreased phase stability known from advanced steels and massive solid solution strengthening of high-entropy alloys. The new dual-phase high entropy alloy (TRIP-DP-HEA) will have improved resistance to intergranular and intergranular sliding, as well as increased strength. The increased strain hardening capacity, which is provided by dislocation hardening of the stable phase and the hardening of the metastable phase, caused by transformation, provides increased ductility. This combined increase in strength and ductility sets TRIP-DP-HEA apart from other newly developed structural materials. [4]. This work is devoted to the study of a two-phase high-entropy as-cast alloy AlFeCoNiCu. The major challenge for the practical applications of the AlFeCoNiCu alloys is their low strength due to the low thermal stability of the alloy microstructure.

High-entropy alloys in the liquid state have low viscosity and, as a result, high atomic mobility, which provides better mixing of the components in the melt, and during crystallization, gives a chaotic distribution of phases in the ingot [5]. Fe, Co, Ni, and Al are evenly distributed within the alloy while Cu tends to segregate in the interdendritic region. [6-8]. The aluminum (Al) additive in AlFeCoNiCu alloy can not only increase the lattice distortion and its elastic energy but also contribute to the formation of the body-centered cubic (BCC) phase. The copper (Cu) additive in AlFeCoNiCu alloy can stabilize the face-centered cubic (FCC) phase and improve the hardness, ductility, and wear resistance [9-11]. It has been that the Cu additive can reduce the wear rate of the $FeCoNiCu_xCr$ alloys significantly due to the self-lubricating mechanism [12]. The $Co_{25}Ni_{25}Fe_{25}Al_{7.5}Cu_{17.5}$(at.%) alloy describes which can contain a single FCC phase under normal casting conditions [13]. The experiments have demonstrated that the crystallographic structures of the $FeCoNi(CuAl)_x$ alloys are transformed from a single face-centered cubic (FCC) phase for $0\leq x\leq 0,6$ to a body-centered cubic (BCC) phase in combination with a minor FCC phase for $0,9\leq x\leq 1,2$, while the FCC plus BCC duplex phases are in the range of $0,7\leq x<0,9$ [14]. The microstructure of the $FeCoNi(CuAl)_{0.8}$ alloy demonstrates the large amounts of a Cu-rich nano-segregations FCC phase dispersed in the BCC matrix. The annealing can lead to the phase transition from FCC to BCC for the $FeCoNi(CuAl)_{0.8}$ alloys. The level of Cu-segregation in $FeCoNi(Cu_mAl)_x$ alloys determines the phase evolution within the inhomogeneous single-phase ($0.75 \leq m < 1.0$), duplex- phase

(m<< 0.75), and triple- phase (m ≈ 0.75) [15]. The Ab-initio molecular dynamics (AIMD) simulations in the AlFeCoNiCu as-cast alloy with equiatomic composition have indicated a possible coexistence of FCC and BCC phases at room temperature and the stabilization of a single FCC phase above 1070 K. The calculated phase diagrams have demonstrated the formation of FCC and BCC phases at room temperature and one FCC phase at a temperature of about 1010 K [16]. The AIMD simulation results showed that the equiatomic phases AlFeCoNi (BCC) and FeCoCu (FCC) are not stable at elevated temperatures. AIMD simulation results predicted a solid-state phase transformation from a two-phase (FCC + BCC) structure to a single-phase FCC structure as the temperature rises to 1073 K. Increasing the amounts of Cu, Ni and Co stabilized the FCC structure instead of the duplex (FCC+BCC) structure. High- temperature XRD (HTXRD) analysis has shown that the weight fraction ratio of FCC to BCC phase increases at 1173K, but about 10% of the BCC phase remains in the system at this temperature [16]. It was found that the coatings of AlFeCoNiCu HEA coatings prepared by gas tungsten arc (GTA) cladding on low-carbon substrates both have BCC dendrites and inclusions of FCC phase in interdendrite area [17].

The AlFeCoNiCu alloy of equiatomic composition in addition has the highest entropy of mixing which results in stability of solution phases [18]. In AlFeCoNiCu alloys, 3d iron is the solvent and forms the matrix phase (primary phase) due to its high melting temperature and relatively large atomic radius [19]. Different constituent elements cause lattice distortion. This lead to an increase in the hardness of the solution and decrease in the degree of crystalline and X-ray scattering [20]. [10, 21]. The addition of nickel to HEA reduces the brittleness during solidification [22]. The results show that the Ni element could lead to the evolution from face- centered cubic (FCC), body -centered cubic (BCC) and ordered BCC coexisting phase structure to a single FCC phase. The change of phase constitution enhances the plasticity but reduces the hardness and strength [23]. The alloy $Al_{10}(FeCoNiCu)_{90}$ was fabricated by mechanical alloying of the powder mixture followed by sintering. A homogeneous powder mixture has obtained after 80 hours of the ball mill. The 80 h-milled powder is crystallized in two face-centered cubic (FCC) phases at the lattice parameters are 3.60 Å and 5.21 Å. The microstructure of the alloy as cast shows spinodal decomposition. The ingot crystallizes in a single-FCC structure and 3.66 Å is the lattice parameter of the corresponding FCC structure [24]. Ferromagnetic moments of iron, cobalt and nickel also provide high magnetic properties of the alloy [25]. The addition of copper stabilizes the FCC phase and increases the ductility of the alloy [26]. The addition of aluminum has also a positive effect on the alloy's properties. A decrease in the density and an increase in the hardness and strength of the alloys is due to increase of the lattice strain, elastic energy, and BCC phase ratio [27]. In addition, the segregation of elements can be done by adding aluminum from dendritic and interdendritic regions [28].

For the $Al_xCu_yFeCrNiCo$ ($0.0 \le x \le 1.5$, $0.5 \le y \le 2$) high entropy alloys different structures (two FCC and one BCC) were detected using X-ray diffraction technique with presence and stoichiometry dependent on the Al and Cu concentrations. Rich Cu and FeCrNiCo phases having FCC structures with different lattice parameters were identified. Phases with a high content of aluminum, nickel, and chromium have a bcc lattice structure with similar parameters. An increase in the Al content led to the disappearance of the FeCrNiCo-rich phase and the appearance of phases rich in Cr and AlNi [29]. AlxCoCrCuFeNi high entropy alloy microstructure change (x = 0.5, 1.5 and 3.0) with increasing Al concentration occurs from one FCC phase to FCC + BCC phase mixture and then to one BCC phase. In addition, an increase in the content of the Al element promotes an increase in hardness, and more significantly in the BCC phase than in the FCC phase. This is due to the fact that the Al element gives a greater strengthening of the solid solution in the BCC phase due to the larger elastic modulus mismatch [30]. The Cu-rich nano twins a face-centered-cubic (FCC) structure were formed in the AlFeCoNiCu high-entropy alloy produced by melt-spinning. The hardness and elastic modulus change with the size of the twin, which is confirmed by the nanoindentation method [31].

This work is devoted to the study of the thermal stability and thermal expansion behavior of AlFeCoNiCu as-cast high- entropy dual-phase alloy, obtained by vacuum arc melting. AlFeCoNiCu as- cast high- entropy alloy with an equiatomic composition was studied by differential scanning calorimetry (DSC) and dilatometry. Phase transformation is one of the essential topics in the studies on high entropy alloys (HEAs). The present work can help in a deep understanding of the phase stability for HEAs. The selection and thermal stability of phases are important in the design of high entropy alloys (HEA).

EXPERIMENTAL SECTION

Materials and fabrication

The samples of the AlFeCoNiCu as-cast high-entropy alloy with equiatomic composition were obtained by vacuum arc melting in the laboratory. The high-purity metals were used as starting materials: aluminum A999 99.9%, copper Mk00 (99.98%), cathode cobalt (99.98%), nickel N-1 (99.98%), and high-purity carbonyl iron 99.98%.

Characterization and measurement

Metallographic investigation of the structure of the AlFeCoNiCu as-cast high-entropy alloy with equiatomic composition was carried out by conventional methods. AlFeCoNiCu samples were obtained in the laboratory and the metal cooling rate was 10 K/s. Neophot32 optical microscope (Carl Zeiss, Germany) was used. The optical microscopic study was carried out for the samples both after etching (3% HNO3 solution in alcohol) and without etching. Microhardness (HV) were measured by a PMT-3 micro hardness tester (Russia). The measuring error HV was 5%. The micro hardness values were averaged over ten measurements. The mechanical properties (Young's modulus E, hardness H) were measured by nanoindentation method using NanoScan-4D (FSBI "TISNCM", Russia) following requirements of ISO 14577. The measurements were performed under continuous loading conditions with a linearly increasing load up to 50 mN at room temperature. The loading and unloading of the indenter, as well as the recording of the P-h diagram (applied load – depth of the indention), were carried out automatically. The hardness and Young's modulus of dendrites were determined because of 50 measurements for each of the regions. The size of the indenter footprint was measured at a maximum depth of indenter. The method of Oliver and Farah was used to process the results of mechanical material testing [32]. The metallographic study and measurement of the surface distribution of elements were carried out by SEM-EDS using a Merlin scanning electron microscope (Carl Zeiss, Germany) equipped with an X-MaxNX-ray energy dispersive spectrometer (Oxford Instruments, UK). The data were collected and analyzed by the Aztec software (Oxford Instruments, UK). SEM was used to visualize the surface morphology and structural defects in the secondary electron mode with a resolution up to 2nm.

Differential scanning calorimetry (DSC) and dilatometry were used to study the thermal stability of as-cast AlFeCoNiCu high entropy alloy with equiatomic composition. Conventional thermal analyses were carried out using an STA 409 PC/PG differential scanning calorimeter (NETZSCH, Germany). TGA and DSC curves of the AlFeCoNiCu alloy were acquired at a heating rate of 5 K/min in the temperature range of 300–1370 K in an argon atmosphere with a flow rate of 30 ml/min. The coefficient

of thermal expansion (CTE) was measured between 300 and 1370 K using a DIL 402 C dilatometer (NETZSCH, Germany) at a heating rate of 5 K/min in an argon atmosphere with a flow rate of 50 ml/min.

RESULTS AND DISCUSSION

Metallographic analysis

The metallographic observation has indicated the dendritic microstructures typical of the as-cast AlFeCoNiCu alloys, i.e. the presence of a large amount of a dendritic BCC phase and an interdendritic FCC phase. According to data [11], the Bragg peaks in the XRD pattern of the AlFeCoNiCu as-cast alloy correspond to simple FCC and BCC phases, the higher peak intensity of the BCC phase suggests it is the dominating phase in the alloy. **Fig. 1** shows the solidification process of the melt AlFeCoNiCu at a cooling rate of 1 - 10 K/s. There are three obvious chemical orders in the AlFeCoNiCu melt: Co - Ni, Cu - Fe, and Al - Fe. Co, Ni, and Cu tend to form the FCC phase, and Al and Fe tend to form the BCC phase. In the region with a high content of Co and Ni, it is easier to nucleate; therefore, at the initial stage of crystallization, the FCC phase is more stable than the BCC phase. The presence of Cu in the FCC phase results in a higher Gibbs free energy. The BCC phase is more stable during the crystallization process. The ingot AlFeCoNiCu is composed of BCC phase Al-rich and FCC phase Cu-rich. These results are in good agreement with the experimental results [33].

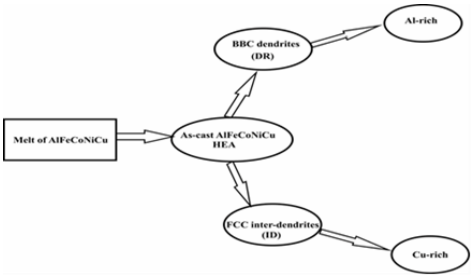

Fig. 1 Solidification process of the melt AlFeCoNiCu at a cooling rate of 1-10 K/s

SEM micrographs presented in **Fig. 2** showed two randomly distributed phases (α and β). BCC (marked as "β" in Figure 2) phase and FCC (marked as "α" in Figure 2) phase were identified earlier by XRD at room temperature [16]. The crystal structures that formed in the alloy system have been determined. The next question is how the alloying elements are distributed between the different phases. **Figure 3** shows the elemental EDS map of equiatomic AlFeCoNiCu alloy providing a qualitative representation of the distribution of elements in each phase. The chemical composition of phases characterized by EDS analysis showed that Fe and Co are almost uniformly distributed in both phases compared to the other elements (**Fig. 3**). The Ni and Al concentrations are higher in the BCC (β) phase than in the Cu-rich FCC (α) phase. This confirms the experimental results, which showed that Al stabilizes the BCC phase, while Cu FCC phase [34, 35]. EDS-analysis demonstrates Cu segregation in the interdendritic (ID) region and the enrichment by other elements in the dendritic region (DR) (**Fig. 3**, **Table 1**), which is consistent with previous reports [7-8, 16]. The positive enthalpy of mixing for Fe - Cu, Co - Cu, Ni - Cu, and Al - Cu explains the precipitation of the Cu rich phase in the BCC DR region. All as-cast AlFeCoNiCu high-entropy alloys consist of a dominating BCC phase and a small amount of FCC phase.

Optical microscopy after chemical etching of the surface revealed many phases in the dendrites and interdendritic space (**Fig. 4**). Different phases vary dramatically in HV Vickers microhardness (MPa). Based on the microhardness data, the phase composition of dendrites and inter-dendritic space is rather complex. For example, the microhardness changes from the peripheral to the center of the dendrite from 2834 to 3050 MPa. The microhardness of inclusions in the interdendritic space differs significantly: 3511, 2187, and 2932 MPa. The ability to design alloys with the desired characteristics provides an accurate characterization of the local mechanical properties of the various phases. In this paper, the nanoindentation method was used to measure the hardness and elastic modulus of different phases in the as-cast AlFeCoNiCu Our measurement results of hardness and elastic modulus values for inter dendrites (ID) and dendrites (DR) of as-cast AlFeCoNiCu alloy are shown in **Table 1** and **Fig. 4**.

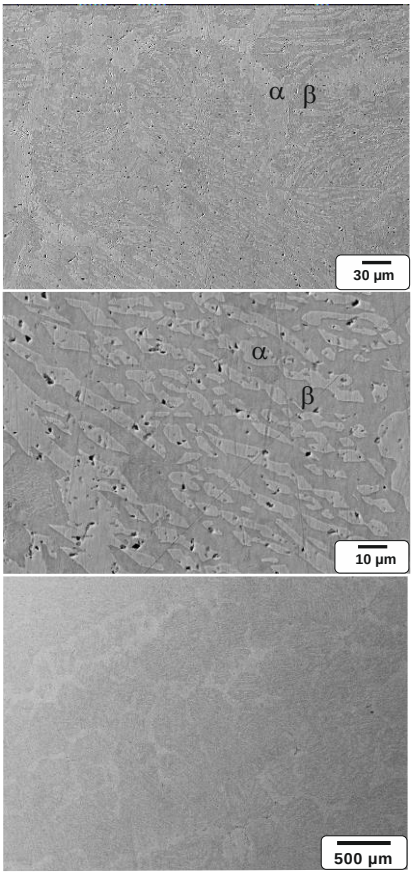

Fig. 2 SEM micrographs of the as-cast AlFeCoNiCu, obtained with back-scattering electron

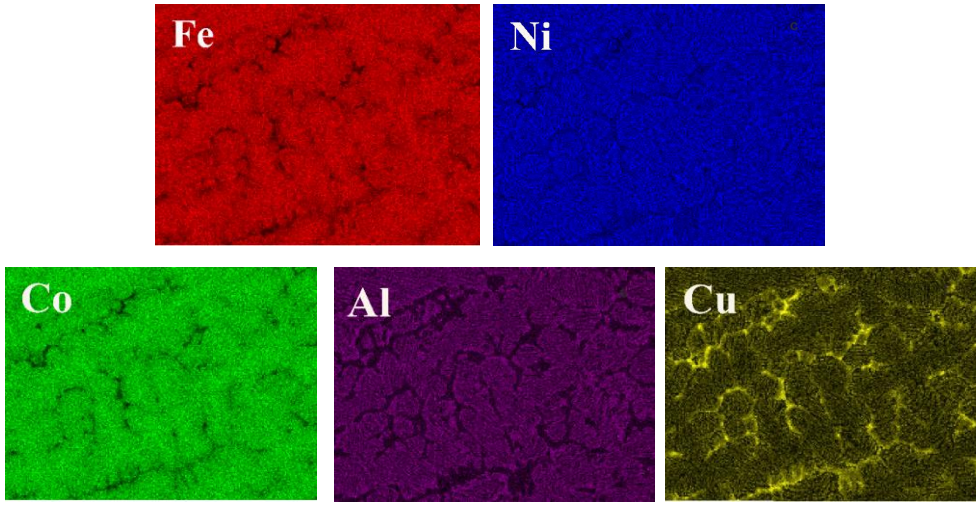

Fig. 3 EDS elemental map of equiatomic AlFeCoNiCu

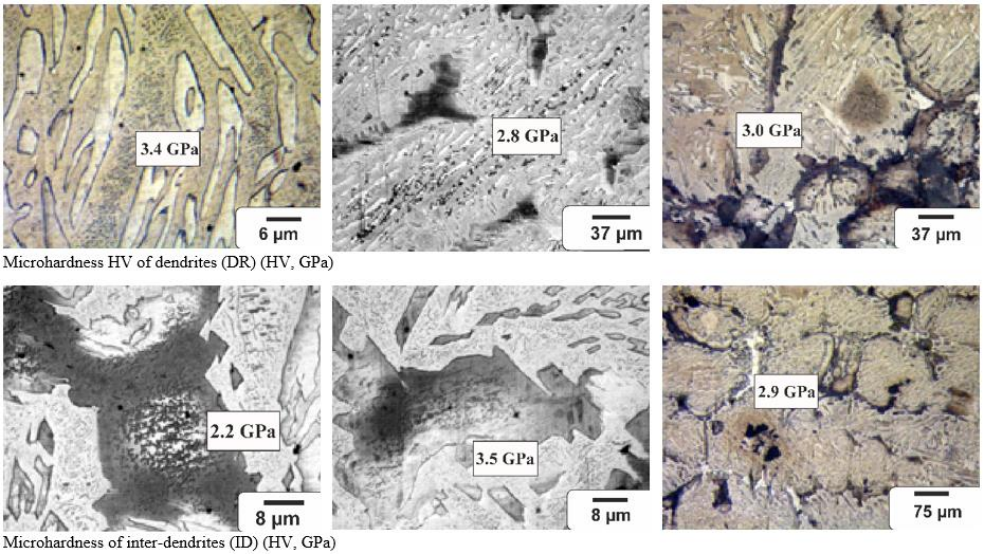

Fig. 4 The microstructure of AlFeCoNiCu alloy ingots (optical microscopy)

Table 1 Hardness and indentation elastic modulus values of AlFeCoNiCu as-cast HEAs

	Inter Dendrites (ID)	Dendrites (DR)
Nanohardrness, HV, GPa	3.4±0.4	4.1±0.6
Microhardness, HV, GPa	(2.2 – 3.5) ±0.4	(2.8 – 3.4) ±0.7
Elastic modulus, E, GPa	130.5±2.0	166.5±5.6

Differential scanning calorimetry

Fig. 5 demonstrates the differential scanning calorimetric (DSC) curve of AlFeCoNiCu as-cast alloy obtained at a heating rate of 5 K/min. The exothermic line in the temperature range from about 800 K to point (A) is apparently related to relaxation of internal stresses in the alloy (structural and lattice deformation). This phenomenon has also been observed in high-entropy alloys of the AlCrFeCoNiCu [26]. Peaks (B) and (C) on the DSC curve observed in the temperature range 1100–1400K are due to solid-phase transformations. As noted above, the Cu-rich phase is precipitated from the dendritic matrix, and the Cu-rich interdendritic phase becomes discontinuous at a temperature above 973K [11]. These phase transformations could be due to the thermally induced dissolution of the solid solution of Cu-rich interdendritic phase in the matrix and the concomitant precipitation of

the new Cu-rich phase from their dendritic matrix [26]. Studies of the DSC curve of the AlFeCoNiCu as-cast alloy (Fig.5) are consistent with the results obtained in work [11] at a heating rate of 10 K/min in the range of 600-1600 K.

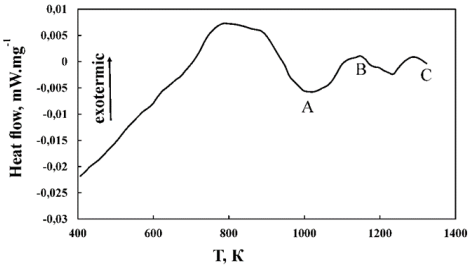

Fig. 5 DSC curve of the AlFeCoNiCu as-cast high-entropy alloy (sample heating rate is 5 K/min.)

Thermal expansion

The thermal expansion of the AlFeCoNiCu as-cast high-entropy alloy was measured by a horizontal push-rod dilatometer in the temperature range from 300K to 1370K. The relative length change of the sample $\Delta l = (l_\tau - l_0)/l_0$ of the AlFeCoNiCu as-cast high-entropy alloy as a function of temperature is almost linear (**Fig. 6a**). The coefficient of thermal expansion (CTE) is $(1/l_\tau)(d(l_\tau - l_0)/dt$ (**Fig. 6b**).

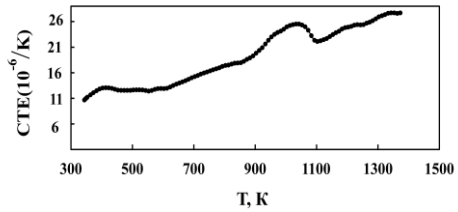

Fig. 6a The relative length change of the sample $\Delta l = (l_\tau - l_0)/l_0$ as a function of temperature for the as-cast AlFeCoNiCu high-entropy alloy

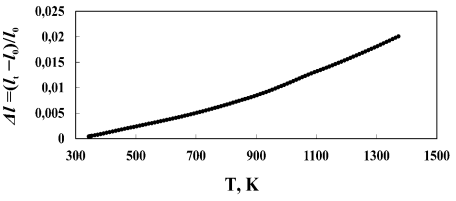

Fig. 6b Dependence of the coefficient of thermal expansion on the temperature for the AlFeCoNiCu as-cast high-entropy alloy

The CTE of the AlFeCoNiCu as-cast high-entropy alloy (Fig.6b) is relatively high as compared to conventional stainless steel, which usually has a CTE from $14 \cdot 10^{-6}$ K^{-1} to $16 \cdot 10^{-6}$K^{-1} [38], and increases linearly with temperature. Such CTE dependence on temperature indicates that the AlFeCoNiCu as-cast high-entropy alloy has good stability at high temperatures from 300K to 1370K (Fig.6a). There is an increase in CTE increase from $(10.6 \pm 0.3) \cdot 10^{-6}$K^{-1} at a temperature of 300K to $(27.7 \pm 0.3) \cdot 10^{-6}$K^{-1} to a temperature 1370 K The peaks in the CTE temperature curve (Fig. 6b) and DSC curve (**Fig. 5**) suggest the phase transformation for AlFeCoNiCu as-cast high-entropy alloy with increasing temperature up to ~1000K. The peaks on the CTE temperature curve correspond to phase transitions. For example, abrupt compression occurs as heated iron-based materials undergo a ferrite-to-austenite transition, which is because the crystal lattice changes from a BCC to a more compact FCC structure [39]. The reference literature data on the thermal expansion of the AlFeCoNiCu as-cast high-entropy alloy are unknown authors of this study. The obtained results were compared with existing literature for AlFeCoNiCu high-entropy alloys [38, 40, 41]. The average CTE of $FeCoCrNi_2Al$ and $FeCoCrNiAl_{0.3}$ up to 1470K is $(15.16 \pm 0.25) \times 10^{-6}$ K^{-1} and $(15.72 \pm 0.35) \times 10^{-6}$ K^{-1}, respectively [40]. The average CTE for HEAs varies from 13.8×10^{-6} K^{-1} to 15.5×10^{-6}K^{-1} at 1270K. The CTE versus temperature plots for the $FeCoCrNiAl_{0.3}$ and NiCoCrAlSi HEAs show a decreasing trend in the temperature ranges of 1170 -1470K and 970 K – 1220K, respectively. An increase in the CTE with increasing temperature up to 1470K is observed for FeCoCrNiAl HEAs [40]. The anomalous CTE was reported for the CoCrFeAl HEA at high temperatures [41], where the temperature dependence of the linear CTE was measured up to 820K. The CTE of the CoCrFeAl alloy demonstrates two deviations from regular behavior: (1) at 430 K - 720K, where the CTE remains almost constant, the anomaly arises due to the ferromagnetic to paramagnetic (FM-PM) phase transition; and (2) at 720 K - 770K, where the CTE decreases with increasing temperature, reaching almost zero at around 770K.

Meanwhile, the sample length stays almost constant in the range of 760–775K, which resembles the Invar effect. The second anomaly should be interpreted as the paramagnetic (PM) to non-magnetic (NM) phase transition [41]. Previously, the kinetics of the phase transformation of FCC to BCC during heating of a high-entropy Al0.5CoCrFeNi alloy was investigated by the thermal expansion method. It was found that the fraction of the FCC phase that has passed into the BCC phase, the activation energy of the phase transformation on heating increases, which indicates an increase in the potential barrier. The phase transition from FCC to BCC is controlled by the rate of nucleation and diffusion across the interface [42].

The possible coexistence of the FCC phase and a body-centered cubic BCC phase at room temperature and stabilization of a single FCC phase above 1070 K at the equiatomic composition of AlFeCoNiCu alloy was also confirmed by the AIMD results [16]. The as-cast high-entropy alloys $Al_xFeCoNiCuCr$ (x = 1.0, 1.5, 1.8) were investigated by means of X-ray diffraction and dilatometric methods. Two-phase condition in the high-entropy alloy and the increase of the crystal lattice parameter of the FCC and BCC phases were detected. For these AlFeCoNiCuCr alloys, the average thermal expansion coefficient $<\alpha> = 12.4 \cdot 10^{-6}$ K^{-1} in the temperature range of 135-545 K were determined [43].

CONCLUSIONS

The AlFeCoNiCu as cast high-entropy alloy has demonstrated a typical cast dendritic microstructure predominantly consisting of BCC and FCC solid solutions. The ingot is composed of the BCC phase and FCC phase, the BCC phase contains more Al, and the FCC phase contains more Cu. EDS-analysis demonstrates Cu segregation in the interdendritic (ID) region and the enrichment by other elements in the dendritic region (DR). Optical microscopy revealed the presence of multiple phases in dendrites and interdendritic space. Based on the microhardness data, the phase composition of dendrites and inter-dendritic space is rather complex. The hardness and modulus of elasticity of two phases BCC and FCC in the high-entropy alloy AlFeCoNiCu were measured for the first time by the nanoindentation

method. Our measurement results of hardness and elastic modulus values for inter dendrites (FCC phase) and dendrites (BCC phase) of as-cast AlFeCoNiCu alloy showed the difference between there. Hardness values for inter dendrites and dendrites: 3.4±0.4GPa and 4.1±0.6GPa. Elastic modulus values for inter dendrites and dendrites: 130.5±2.0GPa and 166.5±5.6GPa. The thermodynamic properties of the as-cast AlFeCoNiCu alloy studied by measuring the coefficients of thermal expansion (CTE) and DSC indicate the change in phase composition on heating to ~1000 K. The coefficient of thermal expansion (CTE) increases linear from $(10.6 \pm 0.3)\times10^{-6}K^{-1}$ at room temperature to $(27.7 \pm 0.3) \times10^{-6}K^{-1}$ at 370K. CTE temperature dependences and DSC results obtained in this study can be useful for quantifying the fundamental aspects such as solid solution strengthening, as well as for structural analysis or design.

Acknowledgments: The work was performed using the equipment of the UCKP "Modern Nanotechnologies" of the Ural Federal University.
This work was supported by state work № FEUZ-0836-0020.

REFERENCES

1. E.P. George, W.A. Curtin, C.C. Tasan: Acta Materialia, 188**,** 2020, 435-474. https://doi.org/10.1016/j.actamat.2019.12.015.
2. D.B. Miracle, O.N. Senkov: Acta Materialia, 122, 2017, 448-511. https://doi.org/10.1016/j.actamat.2016.08.081.
3. T.R Paul, I.V. Belova, G.E. Murch: Materials Chemistry and Physics, 210**,** 2018, 301-308.
https://doi.org/10.1016/j.matchemphys.2017.06.039.
4. Z Li, K.G Pradeep, Y. Deng, D. Raabe, C.C. Tasan: Nature, 534, 2016, 227-300. https://doi.org/10.1038/nature17981.
5.Y. Zhang, Y.J. Zhou, J.P. Lin, G.L. Chen, P.K. Liaw: Advanced Engineering Materials, 10(6), 2008, 534-538. https://doi.org/10.1002/adem.200700240.
6. T. Wang, J. Kong, B. Chao: Fenmo Yejin Jishu /Powder Metallurgy Technology, 29, 2011, 435-438. https://doi.org/10.1002/adem.200700240.
7. O.A. Chikova, D.S. Chezganov, V.S. Tsepelev, V Yu. Ilyin: IOP Conference Series: Materials Science and Engineering, 699, 2019, 012007.
https://doi.org/10.1088/1757-899X/699/1/012007.
8. O. Chikova, V. Tsepelev, V. V'yukhin, K. Shmakova, V. Il'in: Acta Metallurgica Slovaca, 25(4), 2019, 259-266. https://doi.org/10.12776/ams.v25i4.1358.
9. Y.X. Zhuang, W.J. Liu, Z.Y. Chen, H.D. Xue, J.C. He: Materials Science and Engineering A, 556, 2012, 395-399. https://doi.org/10.1016/j.msea.2012.07.003.
10. Y. Zhuang, W. Liu, P. Xing, F. Wang, J. He: Acta Metallurgica Sinica (English Letters), 25, 2012, 124-130. https://doi.org/10.11890/1006-7191-122-124.
11. Y.X. Zhuang, H.D. Xue, Z.Y. Chen, Z.Y. Hu, J.C. He: Materials Science and Engineering A, 572, 2013, 30–35. https://doi.org/10.1016/j.msea.2013.01.081.
12. A. Verma, P. Tarate, A.C. Abhyankar, M.R. Mohape, D.S. Gowtam, V.P. Deshmukh, T. Shanmugasundaram: Scripta Materialia, 161, 2019, 28–31. https://doi.org/10.1016/j.scriptamat.2018.10.007.
13. Z. Fu, W. Chen, H. Wen, D. Zhang, Z. Chen, B. Zheng, Y. Zhou, E.J. Lavernia: Acta Materialia, 107, 2016, 59-71. https://doi.org/10.1016/j.actamat.2016.01.050.
14. Q. Zhang, H. Xu, X.H. Tan, X.L. Hou, S.W. Wu, G.S. Tan, L.Y. Yu: Journal of Alloys and Compounds, 693, 2017, 1061-1067. https://doi.org/10.1016/j.jallcom.2016.09.271.
15. Q. Yu, W-W Xu, C. Cui, X. Gong, W. Li, L. Chen, X. Li, L. Vitos: Journal of Alloys and Compounds, 843, 2020, 156109. https://doi.org/10.1016/j.jallcom.2020.156109.
16. Kivy M. Beyramali, Zaeem M. Asle, S. Lekakh: Materials & Design, 127, 224–232, 2017. https://doi.org/10.1016/j.matdes.2017.04.086.
17. Q. Fan, C. Chen, C. Fan, Z. Liu, X. Cai, S. Lin, C Yang: Surface and Coatings Technology, 420, 2021, 127364. https://doi.org/10.1016/j.surfcoat.2021.127364.
18. Yeh J-W: JOM, 65, 2013, 1759-1771.
https://doi.org/10.1007/s11837-013-0761-6.
19. É. Fazakas, V. Zadorozhnyy, D. Louzguine-Luzgin: Applied Surface Science, 358(B), 2015, 549-555. https://doi.org/10.1016/j.apsusc.2015.07.207.
20. A. Pogrebnjak, A.A. Bagdasaryan, I. Yakushchenko, V.M. Beresnev: Russian Chemical Reviews, 83(11), 2014, 1027. https://doi.org/10.1070/RCR4407.
21. F. Wang, Y. Zhang: Materials Science and Engineering A, 496 (1-2), 2008, 214-216. https://doi.org/10.1016/j.msea.2008.05.020.
22. H.R. Sistla, J.W. Newkirk, F.F. Liou: Materials & Design, 81, 113-121, 2015.
https://doi.org/10.1016/j.matdes.2015.05.027.
23. C. Liu, W. Peng, C.S. Jiang, H. Guo, J. Tao, X. Deng, Z. Chen: Journal of Materials Science and Technology, 35(6), 2019, 1175-1183. https://doi.org/10.1016/j.jmst.2018.12.014.
24. S. Das, S.K. Nishad, P.S. Robi: Physica Status Solidi A – Applications and Materials Science, 218 (8), 2021, 2000825. https://doi.org/10.1002/pssa.202000825.
25. M. Alde´ n, S. Mirbt, H.L. Skriver, N. Rosengaard: Physical Review **B**: Condensed Matter and Materials Physics, 46, 1992, 6303-6312. https://doi.org/10.1103/PhysRevB.46.6303.
26. N. Krapivka, S. Firstov, M. Karpets, A.: Physics of Metals and Metallography, 116(5), 2015, 467-474. https://doi.org/10.1134/s0031918x15030084.
27. O. Senkov, S. Senkova, C. Woodward: Acta Materialia, 68, 2014, 214-228. https://doi.org/10.1016/j.actamat.2014.01.029.
28. K. Zhang, Z. Fu, J. Zhang, W. Wang, H. Wang, Y. Wang, Q. Zhang, J. Shi: Materials Science and Engineering A, 508 (1-2), 2009, 214-219. https://doi.org/10.1016/j.msea.2008.12.053.
29. K. Matusiak, K. Berent, M. Marciszko, J. Cieslak: Journal of Alloys and Compounds, 790, 837-846, 2019. https://doi.org/10.1016/j.jallcom.2019.03.162.
30. Y. Sun, P. Chen, L. Liu, M. Yan, X. Wu, C. Yu, Z. Liu: Intermetallics, **93,** 2018, 85–88.
https://doi.org/10.1016/j.intermet.2017.11.010.
31. P.F. Yu, H. Cheng, L.J. Zhang, H. Zhang, M.Z. Ma, G. Li, P.K. Liaw, R.P. Liu: Scripta Materialia, 114, 2016, 31-34. https://doi.org/10.1016/j.scriptamat.2015.11.032.
32. W.C. Oliver, G.M. Pharr: Journal of Materials Science, 19**,** 2004, 3-20. https://doi.org/10.1557/jmr.2004.19.1.3.
33. S. Guo, Y. Zhang, H. Chen, X .Li, M. Wang: Vacuum, 184, 2021, 109953. https://doi.org/10.1016/j.vacuum.2020.109953.
34. C.C. Tung, J.W. Yeh, T.T. Shun, S.K. Chen, Y.S. Huang, H.C. Chen: Materials Letters, 61(1), 2007, 1-5. https://doi.org/10.1016/j.matlet.2006.03.140.
35. J.M. Wu, S.J. Lin, J.W. Yeh, S.K. Chen, Y.S. Huang, H.C. Chen: Wear, 261(5-6), 2006, 513-519. https://doi.org/10.1016/j.wear.2005.12.008.
36. S. Singh, N. Wanderka, B.S. Murty, U. Glatzel, J.Banhart: Acta Materialia, 59(1), 2011, 182–190. https://doi.org/10.1016/j.actamat.2010.09.023.
37. M. Dada, P. Popoola, N. Mathe, S. Adeosun, S. Pityana: International journal of lightweight materials and manufacture, 4(3), 2021, 339-345.
https://doi.org/10.1016/j.ijlmm.2021.04.002.
38. X.L. An, H. Zhao, T. Dai, H.G. Yu, Z.H. Huang, C. Guo, K. Chu Paul, C.L. Chu: Intermetallics, 110, 2019, 106477. https://doi.org/10.1016/j.intermet.2019.106477

39. J.D. James, J.A. Spittle, S.GR. Brown, R.W. Evans: Measurement Science and Technology, 12(3), 2001, 1-15. https://doi.org/10.1088/0957-0233/12/3/201.
40. M. Jadhav, S. Singh, M. Srivastava, G.S. Kumar Vinod: Journal of Alloys and Compounds, 783, 2019, 662-673. https://doi.org/10.1016/j.jallcom.2018.12.361.
41. L. Liu, S. Huang, L. Vitos, M. Dong, E. Bykova, D. Zhang, B.SG. Almqvist, S. Ivanov, J.E. Rubensson, L.K. Varga, B. Varga, P. Lazor: Communications Physics, 2, 2019, 42. https://doi.org/10.1038/s42005-019-0141-9.
42. J. Wang, S. Niu, T. Guo, H. Kou J. Li: Journal of Alloys and Compounds, 710, 2017, 144-150. https://doi.org/10.1016/j.jallcom.2017.03.249.
43. V.M. Nadutov, S.Yu. Makarenko, Ye.O. Svystunov: Metallofizika i Noveishie Tekhnologii, 37, 2015, 987-1000. https://doi.org/10.15407/mfint.37.07.0987.